

transfer atoms from the 3D_J states into the 1D_2 state, from which they can be excited to the $^1P_1^o$ state, returning them to the cooling cycle.

Of the four transitions involved, the $^3F_2^o \rightarrow ^1D_2$ and the $^3F_2^o \rightarrow ^3D_3$ transitions have not been experimentally observed before [9, 10]. This necessitated a spectroscopic study of the $^3F_2^o$ state, which involved measuring the oscillator strengths of the transitions to this state from the relevant D -states and the respective branching ratios.

Precise measurements of oscillator strengths and the branching ratios provide effective tests of atomic structure calculations, especially where electron correlation effects [11] and relativistic corrections [12] are important. They are also important for atomic parity non-conservation searches in the unified electro-weak theories [13]. Oscillator strengths can be determined either directly or indirectly. Direct measurements rely on absolute measurements of absorption, emission, or dispersion of relevant transitions, while indirect methods include combined measurements of the branching ratios and the lifetimes of the relevant higher states. Direct measurements require the knowledge of the sample number density as well as local thermodynamic equilibrium [13]. However, since the $^3F_2^o$ state has large branching ratios to several long-lived states, it is suitable for a novel method for measuring the oscillator strengths that circumvent these requirements. This method is described below.

II. METHOD

The method that we employ for measuring the oscillator strengths of the transitions from the different D -states to the $^3F_2^o$ state requires that when ‘probed’ on a certain D -state to $^3F_2^o$ state transition, the atoms scatter only a few photons from the probe laser before they decay into a meta-stable dark state. The lifetimes of the 1D_2 and 3D_1 states are measured to be $385(45) \mu\text{s}$ [14] and $510(60) \mu\text{s}$ [15] respectively, and the calculated lifetime of the 3D_2 state is determined to be 4 s [16]. By comparison, the average transit time of the atoms through the beam is $38 \mu\text{s}$.

For the 3D_3 we set an upper bound on the branching ratio by comparing the fluorescence signal as the atom decays into this state, compared to the fluorescence signal as it decays into the 1D_2 state. For the rest, we selectively ‘probe’ the atoms in the three different states, 1D_2 , 3D_2 and 3D_1 by exciting them into the $^3F_2^o$ state and observing the fluorescence as they decay to one of the other non-probed states. Since we use an atomic beam for our measurements, an atom that decays into an unprobed or “dark”, long-lived D -state, is not re-excited by the probe beam. For instance, the $^3F_2^o$ state decays with a maximum branching ratio of about 60% into the 3D_2 state, which corresponds to on average 2.5 photons/atom scattered on this transition before going dark. The probability with which the atom scatters a probe photon is a Poisson process dependent on the oscillator strength

of the transition, as well as the natural linewidth of the $^3F_2^o$ state, which is proportional to the sum of the oscillator strengths of all its possible decay channels. An atom that decays from the $^3F_2^o$ state to the probe state with a probability p , has a probability of $p^{n-1}(1-p)$ of decaying into a dark state after n scattering events. Here p is the branching ratio from the $^3F_2^o$ state to the probe state and is a function of the oscillator strengths. Thus, the overall process is described by a Poisson and geometric distribution. If we probe all the relevant transitions to the excited state of interest, we can fit for every oscillator strength. We also need to know the oven temperature, although it will be shown later that this does not need to be very precise. It also requires a measurement of the probe beam profile and the probe beam powers. Apart from these, this method circumvents the need for atomic flux calibration and the absolute efficiency of various parts of the experimental setup. As for the $^3F_2^o$ state, this provides an effective technique for oscillator strength measurements in an atomic beam, where one probes a state directly inaccessible from the ground state, and with significant branching ratios to several lower lying, long-lived states.

III. EXPERIMENTAL SETUP

The measurements presented in this work were performed on ^{226}Ra ($t_{1/2} = 1600 \text{ y}$, $I = 0$). The experimental setup is shown in Fig. 2. We load $3 \mu\text{Ci}$ of ^{226}Ra in the form of radium nitrate salt along with two 25 mg pieces of metallic barium into the oven and radiatively heat it. The barium helps chemically separate the radium from the radium salt, allowing a steady flux of atomic radium out of the nozzle. The nozzle geometry limits the divergence of the atomic beam to 50 mrad [6]. About 30 cm from the nozzle, the atoms are excited into the $^1P_1^o$ state using 3 mW of 483 nm ‘pump’ light produced by a Toptica DL Pro diode laser which is frequency stabilized to a zerodur optical cavity. The atoms then decay to the long-lived D -states as shown in the inset of Fig. 2. The probe laser beams at 912 nm, 712 nm and 698 nm for respectively probing the 1D_2 , 3D_2 , and 3D_1 state are produced by a Sirah Matisse Ti:Sapphire ring cavity laser which is frequency stabilized to a high finesse ULE optical cavity. For instance, in Fig. 2, we probe the atoms in the 3D_2 state by resonantly exciting the atoms into the $^3F_2^o$ state with a 712 nm probe beam and observing the subsequent decay of the atoms into the 3D_1 state at 698 nm. We collect line-shape data for a given probe transition and laser power by scanning the probe laser frequency. This is repeated for a range of different probe powers.

We scan the frequency of the probe laser by double passing it through an acousto-optic modulator (AOM) and scanning its input RF frequency. The fluorescence signal is collected by a 2" diameter, 10 cm focal length lens, filtered and focused onto a photo-multiplier tube

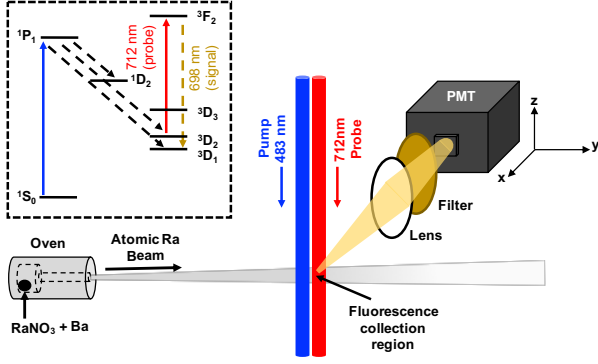


FIG. 2: Spectroscopy measurement setup (not to scale).

The atoms exiting the oven are pumped into the $1P_1^o$ state from which they decay into the D -states. Here, we probe the atoms in the $3D_2$ state with a resonant 712 nm probe laser beam which excites them into the $3F_2^o$ state and the resultant fluorescence 698 nm is filtered and detected on a PMT. Inset: the relevant energy levels and the transitions involved for probing the atoms in the $3D_2$ state and detecting the fluorescence as the atoms decay from $3F_2^o \rightarrow 3D_1$.

(PMT) (Hamamatsu, H7421-50). The PMT output is sent to a data acquisition (DAQ) card (NI- USB6341). The pump laser is shuttered a rate of 0.5 Hz to subtract any scattered background from the probe light on the PMT in the fluorescence signal. This is repeated for all the probe transitions of interest. The probe beam intensity profile is measured using a Thorlabs DCC1545M CMOS camera (1280×1024 pixels).

To limit the branching ratio of the $3F_2^o \rightarrow 3D_3$ transition, with the probe laser at 912 nm, probing the $1D_2 \rightarrow 3F_2^o$ transition, we compare the signal at 750 nm (decay to the $3D_3$ state), with the signal strength at 698 nm (decay to the $3D_1$ state) using narrow bandwidth filters. Using the value we obtain for the 698 nm branching ratio from our analysis, we convert the relative limit on the branching ratio of $3D_1 \rightarrow 3F_2^o$ transition to an absolute limit.

IV. DATA ANALYSIS

We collect lineshape data for 8 different powers with the probe at 712 nm and 5 different powers each with the probe at 698 nm and 912 nm, a total of 18 lineshape data sets. For each of the lineshape data sets measured, we fit the fluorescence counts at the signal transition to a function ‘ F ’ to extract the oscillator strengths:

$$F = A \sum_{n=1}^{n_{\max}} p_{ik}^{n-1} (1 - p_{ik}) [1 - \text{CDF}(\Lambda, n)] + C_0, \quad (1)$$

where n is the number of photons scattered before the atom decays into the signal state, p_{ik} is the branching

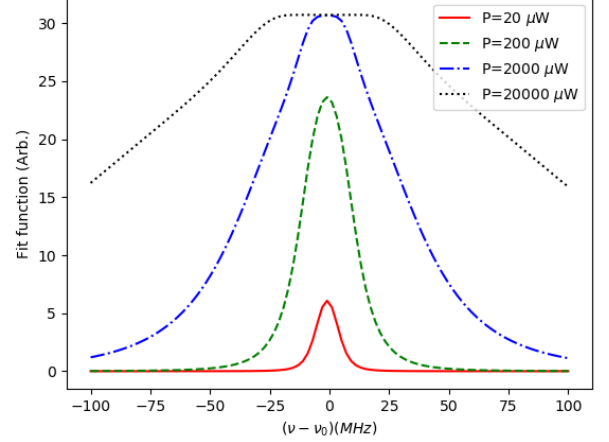


FIG. 3: An example of the behavior of the fit function as the probe beam power is increased. This example is shown for the 712 nm probe transition, which has an oscillator strength $f_{ik} = 0.32(12)$.

ratio from the $3F_2^o$ state to the probe state k , A is an amplitude extracted from the fit, and C_0 is a constant offset. The nominally infinite sum is truncated to n_{\max} and checked for convergence. The term $p_{ik}^{n-1}(1 - p_{ik})$ is the geometric probability that the atom decays into a dark state after on the n^{th} scattering event from the probe state k .

The cumulative distribution function, CDF, for a Poissonian distribution that describes our probing process, is the probability that up to n probe photons are scattered. The term $1 - \text{CDF}$ represents the probability that the probe laser power is sufficient to scatter at least n photons, and the cumulative term $p_{ik}^{n-1}(1 - p_{ik})[1 - \text{CDF}]$ gives the probability that after scattering n probe photons the atom decays into our signal state. The CDF is given by

$$\text{CDF}(\Lambda, n) = \frac{\Gamma[\text{floor}(n+1), \Lambda]}{\text{floor}(n)!}, \quad (2)$$

where Γ is the upper incomplete gamma function. The beam shape is incorporated into the expression for the Poissonian weight, Λ , given by:

$$\Lambda = \sum_y \tau \bar{n}(y) f \sigma_0 g(\nu - \nu_0; \Gamma, \gamma_D), \quad (3)$$

where τ is the interaction time as the atom passes through one pixel of the laser beam image of width Δy , f is the oscillator strength, ν is the laser frequency, ν_0 is the line center, and $\sigma_0 = \pi r_e c = 2.654 \times 10^{-2} \text{ cm}^2/\text{s}$, where r_e is the classical electron radius and c is the speed of light [17]. g is the lineshape function and $\bar{n}(y)$ is the photon intensity at a given y -pixel. The interaction time is determined by the velocity distribution of the beam:

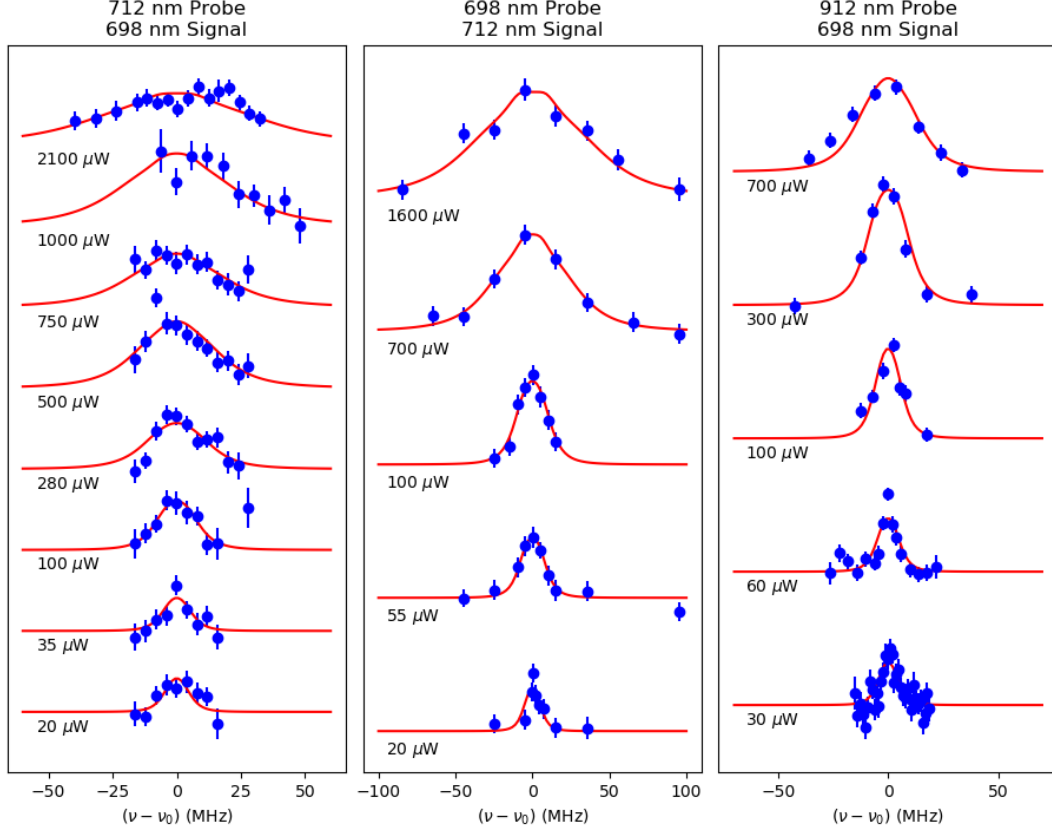


FIG. 4: Waterfall plot of the data and the fits for each of the lineshapes measured in the experiment. The count rate for a particular probe transition at a given power is plotted against the detuning $(\nu - \nu_0)$ from resonance. The lineshapes are offset vertically for clarity.

$$\tau = \Delta y \left\langle \frac{1}{v} \right\rangle \quad (4)$$

$$\left\langle \frac{1}{v} \right\rangle = \int_0^\infty B(v; T) \frac{1}{v} dv, \quad (5)$$

where the Boltzmann velocity distribution $B(v; T)$ is defined as [18]:

$$B(v; T) = 2 \frac{u^2}{\bar{v}} e^{-u^2} \quad (6)$$

$$u = v/\bar{v}, \quad (7)$$

where \bar{v} is the most probable speed.

The photon intensity observed by an atom at horizontal position y , $\bar{n}(y)$ is:

$$\bar{n}(y) = \frac{P}{h\nu\Delta y^2} \frac{\sum_x I(x, y)}{\sum_{x,y} I(x, y)}, \quad (8)$$

where P is the total power in the laser beam, Δy is the width on one pixel on the beam image ($5.2 \mu\text{m}$), and $I(x, y)$ is the beam strength at pixel (x, y) .

The lineshape function $g(\nu - \nu_0; \Gamma, \gamma_D)$ is a Voigt profile, with the Gaussian width γ_D determined, by a measurement of the Doppler-broadened linewidth on the narrow 714 nm, $^1S_0 \rightarrow ^3P_1^o$ transition ($\Gamma_{714} = 2\pi \times 380 \text{ kHz}$), to be 2.32 MHz. The Lorentzian width of the Voigt profile is a dependent parameter of the fit:

$$\Gamma = \sum_i A_{ki} = \frac{2\pi^2 r_e c}{2J_k + 1} \sum_i \frac{2J_i + 1}{\lambda_{ik}^2} f_{ik}, \quad (9)$$

where A_{ki} is the spontaneous decay transition rate from an upper state k to a lower state i , and J_i and J_k are the total angular momenta of states i and k respectively. The branching ratios p_{ik} can be expressed in terms of A_{ki} as:

$$p_{ik} = \frac{A_{ki}}{\Gamma}. \quad (10)$$

The parameters of the fit are the oscillator strengths f_{ik} , the peak amplitudes A , the peak centers ν_0 , and the offsets C_0 . The offsets, peak centers, and oscillator strengths are common for fits of peaks from the same transition. The amplitudes vary between different line-shapes due to variations in the atom flux from the oven. The offsets are to account for various background sources. Examples of the effect of the oscillator strength on the fit function are shown in Fig. 3. As the power increases, it results in a broader peak for a fixed oscillator strength.

The lineshapes for each power taken for each transition are cumulatively fit, using a least squares method using the curve fitter from the scipy library, version 1.1.0, in Python.

V. RESULTS

Fits for each of the lineshapes measured are shown in Fig. 4. The reduced chi-squared for the cumulative fit is $\chi^2_\nu = 1.13$, (179 DOF). Results for the oscillator strengths and branching ratios are shown in Table III. From these oscillator strengths we can determine the linewidth of the $^3F_2^o$ state to be 10.4 ± 2.7 MHz.

Convergence of the sum in Eqn. 1 is tested by varying the upper limit on n , testing the values $n_{\max} = [5, 10, 20, 40]$. Results of this test are shown in Table I. For $n_{\max} = 10$ and above, there is strong convergence for all of the oscillator strengths.

n_{\max}	$^3F_2^o \rightarrow ^3D_2$	$^3F_2^o \rightarrow ^3D_1$	$^3F_2^o \rightarrow ^1D_2$
1	0.247(44)	0.234(39)	0.046(7)
5	0.294(71)	0.254(65)	0.042(7)
10	0.318(105)	0.243(79)	0.041(8)
20	0.318(119)	0.245(87)	0.041(9)
40	0.317(120)	0.245(87)	0.041(9)

TABLE I: Convergence of the oscillator strengths as a function of the number of terms, n_{\max} , in the sum in Eqn. 1.

$T(^{\circ}\text{C})$	$^3F_2^o \rightarrow ^3D_2$	$^3F_2^o \rightarrow ^3D_1$	$^3F_2^o \rightarrow ^1D_2$
420	0.317(120)	0.239(85)	0.040(9)
470	0.318(119)	0.245(87)	0.041(8)
520	0.319(119)	0.251(88)	0.042(9)

TABLE II: The oscillator strengths as a function of the temperature of the Radium oven, with $n_{\max} = 20$.

An additional factor that may affect our results is the temperature of the radium oven source. There can be uncertainty in this temperature due to temperature gradients between inside of the oven crucible and the monitor thermocouple at the rear of the crucible. This would cause a systematic shift in the Boltzmann factor $B(\nu; T)$, which affects the interaction time τ of the atoms with the

laser beam in Eqn. 3. To test this, we fit the data using $n_{\max} = 20$ and $T = [420, 470, 520]^{\circ}\text{C}$. Results of this test are shown in Table II. We find both of these systematic effects to be negligible.

A limit on the $^3F_2^o \rightarrow ^3D_3$ branching ratio was determined by comparing the strength of the signal at 750 nm from this transition to the 3D_1 signal strength at 698 nm. A 105-minute integration of the 750 nm signal level resulted in 2.5 ± 0.75 counts per second, compared to a 10 minute integration at 698 nm, where we had a signal level of 73 ± 2.9 counts per second.

A source of systematic error in this measurement that had to be accounted for is the leakage of 483 nm light through the 750 nm filter. This leakage causes a constant offset on the signal level, which is accounted for in the lineshape fitting by adding a constant offset. In the 750 nm measurement, however, this error can appear as a false detection of atoms decaying on this decay channel. To determine the effect of 483 nm leakage, we measured the PMT signal in the absence of probe light for a period of 14 hours, yielding a signal level of 2.43 ± 0.28 counts per second. After removing this effect, the result at 750 nm is 0.08 ± 0.81 counts per second, which we interpret as an upper limit of 0.4% (68% C.L.) on the branching ratio to 3D_3 . This upper bound is computed using the Feldman-Cousins construction of confidence intervals for a Gaussian distribution constrained to have a non-negative mean. [19]

VI. DISCUSSION

Although differing in detail from the prediction in [8], the overall picture of strong spin-orbit coupling in $^3F_2^o$ is confirmed. The 3D_3 is found to be highly suppressed, and the 1D_2 strongly enhanced compared to the normal dipole selection rules for a $^3F_2^o$ state. The oscillator strength of the 3D_2 channel is found to be significantly higher than predicted, although the others are in good agreement. It should be noted, however, that the $^3F_2^o \rightarrow ^1D_2$ transition is a forbidden transition in the absence of relativistic effects with its branching ratio component coming from the strong spin-orbit interaction in the $^3F_2^o$ state.

For the $^3F_2^o \rightarrow ^3D_3$ transition, the branching ratio from the dipole matrix elements from [8] is 3.6×10^{-4} , which is an order of magnitude below our upper bound of 4×10^{-3} (68% C.I.).

The theoretical value for the lifetime of the $^3F_2^o$ state is 33 ns [8], which differs from our experimental lifetime (derived from the natural linewidth) of 15.3 ± 4.0 ns, by about a factor of two.

Our results for the branching ratios out of the $^3F_2^o$ are promising for the use of this state for our scheme for repumping the blue Zeeman slower. The branching ratio to the 1D_2 state is high enough to make repumping through this state reasonable, despite being lower than the theoretical branching ratio. With a branching ratio

TABLE III: Wavenumbers, Oscillator strengths (f_{ik}), and branching ratios (BR) for the transitions out of the $^3F_2^o$ state. Theory values for the branching ratio from [8] are shown for comparison.

Transition	Wavenumber (cm ⁻¹)	f_{ik} (theory)	f_{ik}	BR
$^3F_2^o \rightarrow ^1D_2$	10956.7095(5)	0.054	0.041(9)	0.050(11)
$^3F_2^o \rightarrow ^3D_2$	14044.0875(5)	0.074	0.32(12)	0.64(24)
$^3F_2^o \rightarrow ^3D_1$	14322.2340(5)	0.202	0.25(8)	0.31(11)

of 0.05, 20 excitations would be needed on average to bring an atom into the 1D_2 state.

VII. CONCLUSIONS

We have measured the oscillator strengths and the branching ratios of the decay channels of the $^3F_2^o$ state. We employ what we believe to be a novel technique that is used in an atomic beam measurement and requires that the atom excited to a higher energy level decays into several long-lived states, and therefore scatters only a few photons on the transition of interest. This technique requires measuring lineshape data for a number of powers for all the transitions involved. The cumulative fit to all the data is a function of the oscillator strengths of all the transitions to the excited state. This method avoids the need for knowledge of the atomic number density, as well as the absolute calibration of the efficiencies of the different parts of the experimental setup.

The systematic effects due to the oven temperature uncertainty and the finite sum over the photon scattering events n in the fit function Eq. 1 up to an upper limit n_{\max} were studied. Both of these effects are negligible compared to the statistical uncertainties in the oscillator strengths. The main limitation on the maximum number

of photons is computation time. Our implementation of the fitting algorithm took about a day to run with $n_{\max} = 40$ on a laptop computer with an Intel i7-7700HQ CPU.

The strong decay channel to 1D_2 , along with the strong suppression of the branching ratio to the 3D_3 state compared to the 1D_2 state supports the theoretical prediction of strong spin-orbit coupling in the $^3F_2^o$ state in radium.

The above spectroscopic study of the $^3F_2^o$ state supports our proposal of using this state as a spin flipping channel for implementing the blue slower upgrade to our atom slowing and cooling apparatus. This will improve our atom trapping efficiency by two orders of magnitude and enhance our sensitivity to the atomic EDM of ^{225}Ra by at least a factor of 10, setting very stringent limits on the hadronic CP -violating parameters.

VIII. ACKNOWLEDGMENTS

This work is supported by the U.S. DOE, Office of Science, Office of Nuclear Physics under contracts DE-AC02-06CH11357 and DE-SC0019455, and by Michigan State University. RR acknowledges support from the United States Department of Energy Office of Science Graduate Student Research (SCGSR) Program.

-
- [1] N. Auerbach, V. V. Flambaum, and V. Spevak, *Phys. Rev. Lett.*, **76** 4316 (1996)
 - [2] V. Spevak, N. Auerbach, and V. V. Flambaum, *Phys. Rev. C*, **56** 1357 (1997)
 - [3] V. A. Dzuba, V. V. Flambaum, J. S. M. Ginges, and M. G. Kozlov, *Phys. Rev. A*, **66** 012111 (2002)
 - [4] J. Dobaczewski, and J. Engel, *Phys. Rev. Lett.*, **94** 232502 (2005)
 - [5] Y. Singh and B. K. Sahoo, *Phys. Rev. A*, **92** 022502 (2015)
 - [6] M. Bishof *et al.*, *Phys. Rev. C*, **94** 025501 (2016)
 - [7] T.E. Chupp, P. Fierlinger, M.J. Ramsey-Musolf, and J. T. Singh, *Rev. Mod. Phys.*, **91** 015001 (2019)
 - [8] V A Dzuba and V V Flambaum, *J. Phys. B: At. Mol. Opt. Phys.*, **40** 227 (2007)
 - [9] U. Dammalapati *et al.*, *J. Phys. Chem. Ref. Data*, **45** 013101 (2016)
 - [10] E. Rasmussen, *Z. Phys.*, **86** 607 (1934)
 - [11] A Hibbert, *Rep. Prog. Phys.*, **38** 1217 (1975)
 - [12] A Hibbert, *Phys. Scr.*, **16** 7 (1977)
 - [13] M C E Huber and R J Sanderman, *Rep. Prog. Phys.*, **49** 397 (1986)
 - [14] W. L. Trimble *et al.*, *Phys. Rev. A*, **80** 054501 (2009)
 - [15] J.R. Guest *et al.*, *Phys. Rev. A*, **98** 093001 (2007)
 - [16] J. Biero *et al.*, *J. Phys. B: At. Mol. Opt. Phys.*, **37** L305 (2004)
 - [17] O. Axner, J. Gustafsson, N. Omenetto, and J. D. Winefordner, *Spectrochim. Acta Part B*, **59** (2004) 1-39
 - [18] D. H. Potterveld *et al.*, *ArXiv:1903.07798* (2019)
 - [19] G. J. Feldman and R. D. Cousins, *Phys. Rev. D*, **57** 3873 (1998)